EXPERIMENTAL VERIFICATION OF DYNAMICS OF A NOVEL MAGNETIC SHOCK ABSORBER

Amirhossein Daliri Shadbad[1,2], Fred F. Afagh,[1], Fidel Khouli[1], Robert G. Langlois[1]
[1]*Mechanical and Aerospace Engineering Department, Carleton University, Ottawa, ON, Canada*
[2]*Email: amirdalirishadbad@cmail.carleton.ca*

ABSTRACT

The aim of this paper is to experimentally validate the nonlinear dynamic modelling of a novel magnetic shock absorber. The shock absorber under investigation consists of multiple identical repelling magnets arranged in a 1D lattice configuration with an electromagnetic coil energy harvesting system. The unknown parameters of the shock absorber, such as magnetic repelling force relation, were identified. The static and transient responses of the simulation were compared with those of the manufactured magnetic shock absorber prototype and it was shown that the simulation and the experimental results are in agreement. Due to the highly nonlinear nature of the system, there are some difficulties inherent in characterizing the shock absorber's behaviour that the present study attempts to overcome.

Keywords: Nonlinear damper; Magnetic lattice; Energy harvesting.

VÉRIFICATION EXPÉRIMENTALE DE LA DYNAMIQUE D'UN NOUVEL AMORTISSEUR MAGNTIQUE

RÉSUMÉ

L'objectif de cet article est de valider expérimentalement la modélisation dynamique non linéaire d'un nouvel amortisseur magnétique. L'amortisseur étudié consiste en de multiples aimants rpulsifs identiques disposés dans une configuration de treillis 1D avec un système de récolte d'énergie par bobine électromagnétique. Les paramètres inconnus de l'absorbeur de chocs, tels que la relation de force de répulsion magnétique, ont été identifiés. Les réponses statiques et transitoires de la simulation ont été comparées à celles du prototype d'amortisseur magnétique fabriqué et il a été démontré que la simulation et les résultats expérimentaux sont en accord. En raison de la nature hautement non linéaire du système, la caractérisation du comportement de l'amortisseur se heurte à certaines difficultés que la présente étude tente de surmonter.

Mots-clés : Amortisseur non linéaire ; Réseau magnétique ; Récolte d'énergie.

1. INTRODUCTION

The important problem of vibration isolation has been studied extensively over the years [1]. Commonly, viscous dampers are used as isolation devices to reduce the adverse effect of external excitation [2]. Since the introduction of magnetorheological (MR) fluid by Rabinow [3], MR dampers have gained in popularity as they enable a variable damping force to be provided in response to an electrical control signal. MR dampers have been developed for various applications such as automotive suspension [4], airplane landing gear systems [5], medical devices [6], and even seismic applications [7]. The novel shock absorber studied in this paper not only could offer the same damping force controlability but also the capability to convert the system's kinetic energy to electric power. Additionally, its nonlinear characteristics could be beneficial in applications such as automotive suspension systems.

In [8], a novel shock absorber design was proposed that could be utilized in ground vehicle applications. The proposed shock absorber consists of a 1D nonlinear lattice of equal strength repelling permanent magnets that are confined between two fixed magnets with a multi-coil setup wrapped around the 1D lattice for energy harvesting, as shown in Fig. 1. The repelling magnets act as a spring element and the coils act as a damping element due to energy dissipation through induced current in the coils. Both the stiffness and the damping are nonlinear, and this nonlineairty arises from the magnetic potential of the permanent magnets and the damping forces due to the induced current in the coils. The shock absorber's stiffness curve is exponential and can be adjusted by varying the magnets' inter-lattice equilibrium distance, magnet grade and size, and magnet count. The damping can be adjusted by altering the electrical resistance of the coils, coil length, and number of coil turns.

In this study, a sample magnetic shock absorber has been manufactured in accordance to the design proposed in [8]. Utilizing the experimental apparatus, the parameters of the prototype system are identified and the nonlinear dynamics of the shock absorber element developed in [8] are validated. The paper is organized as follows. Following the introduction in Section 1, Section 2 briefly describes the derivation of equations of motion (EOM) for the magnetic shock absorber that were detailed in [8]. Section 3 describes the chosen experimental setup and the details of the measurement instruments used. The parameters, such as damping coefficient, of the shock absorber are identified experimentally and the procedure is explained in Section 4. The experimental results and the description of the methods used to verify the simulation are discussed in Section 5. Lastly, conclusions are outlined in Section 6

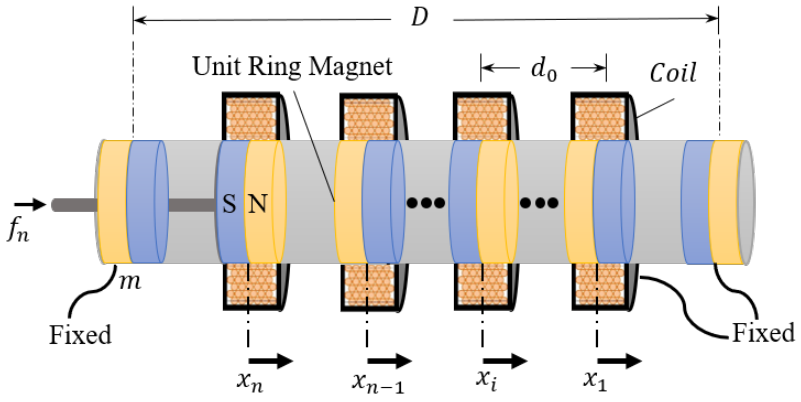

Fig. 1. Schematic of the novel shock absorber.

2. DYNAMICS

With reference to Fig. 1, the system consists of a number of ring magnets arranged in a 1D lattice configuration with axial magnetic polarization and similar physical properties so that the initial distance between adjacent magnets is the same and assumed to be d_0. The magnets at each end are fixed, confining the range of motion of the sliding magnets. With n sliding magnets, the external force is applied to the n^{th} magnet. For each sliding magnet there is a corresponding electromagnetic coil, thus there are n coils as well. Each sliding magnet experiences a force due to its interactions with the adjacent sliding or fixed magnets and an additional force due to its interaction with the coils.

2.1. Magnetic Force

Based on the research conducted by Molerón et al. [9], the repelling force between two adjacent magnets is given by

$$F_{repelling} = Ad^p \tag{1}$$

where $A > 0$ and $p < 0$ are empirically-derived constants and d is the distance between the two magnets. Note that the constants depend on the magnet's properties, such as grade and size. According to [9], since for typical magnets the repelling force diminishes rapidly as the distance increases, the effects of non-adjacent magnets can be ignored.

2.2. Electromagnetic Damping

The repelling magnetic chain alone acts as a nonlinear spring element, ignoring the friction forces between the magnets and the shaft; however, adding electromagnetic coils to the setup enables the dissipation of energy from the system and provides the ability to harvest the kinetic energy of the magnets into electrical energy. This is due to Faraday's law of induction, which states that whenever a conductor loop experiences a change in magnetic flux, an electromotive force will be induced in that loop. The resulting current in the loop in return creates a magnetic field which opposes changes in the initial magnetic field according to Lenz's law [10].

According to Faraday's induction law, the electromagnetic force is proportional to the relative speed of the magnet with respect to the coil. Therefore, electromagnetic energy dissipation is velocity dependant and can be modelled similar to a viscous damper as:

$$F_{e_{ij}} = C_{e_{ij}} \dot{x}_i \tag{2}$$

where $F_{e_{ij}}$ is the electromagnetic damping force exerted on magnet i by coil j, $(1 \leq i, j \leq n)$, $C_{e_{ij}}$ is the damping coefficient due to interaction between magnet i and coil j, and $\dot{x}_i$ is the velocity of i^{th} magnet with the assumption of fixed coils. Unlike a simple viscous damper, the damping coefficient is not constant. According to [11–13] it is dependant on the magnetic field density as given by

$$C_{e_{ij}} = \frac{\left(NB_{ij}l_c\right)^2}{R_{load} + R_{coil}} \tag{3}$$

where N is the number of coil turns, B_{ij} is the average magnetic flux density of magnet i interacting with coil j, l_c is the coil length, R_{coil} is the internal electrical resistance of the coil, and R_{load} is the connected resistive load. Therefore, the total electromagnetic damping coefficient of the i^{th} magnet can be obtained as

$$C_{e_i} = \sum_{j=1}^{n} C_{e_{ij}} \tag{4}$$

Note that unlike the repelling force case where the effect of non-adjacent magnets were ignored, in this case the effects of all coils are considered since a single magnet throughout its travel, due to a perturbation, can come within range of any coil, where the force due to their interaction is significant. Detailed derivation of damping due to coil effects is provided in Reference [8]. Ultimately, the total damping coefficient for each magnet can be given by

$$C_i = C_{e_i} + C_{v_i} \tag{5}$$

where C_{v_i} is the viscous friction coefficient of the i^{th} magnet obtained experimentally. Based on the developed expressions for the repelling and the damping forces, the EOM of the system were obtained using Newtonian dynamics as shown,

$$\begin{bmatrix} m & 0 & \dots & \dots & 0 \\ 0 & \ddots & \ddots & \ddots & \vdots \\ \vdots & \ddots & m & \ddots & \vdots \\ \vdots & \ddots & \ddots & \ddots & 0 \\ 0 & \dots & \dots & 0 & m \end{bmatrix} \begin{Bmatrix} \ddot{x}_1 \\ \vdots \\ \ddot{x}_i \\ \vdots \\ \ddot{x}_n \end{Bmatrix} = \begin{Bmatrix} A(d_0 + x_1 - x_2)^p - A(d_0 - x_1)^p - C_1\dot{x}_1 \\ \vdots \\ A(d_0 + x_i - x_{i+1})^p - A(d_0 + x_{i-1} - x_i)^p - C_i\dot{x}_i \\ \vdots \\ f_n + A(d_0 + x_n)^p - A(d_0 + x_{n-1} - x_n)^p - C_n\dot{x}_n \end{Bmatrix} \tag{6}$$

where m is the mass of each magnet, f_n is the external force applied to the n^{th} magnet, and x_i is the displacement of magnet i from its initial equilibrium position.

3. EXPERIMENTAL APPARATUS

For experimental purposes, a lattice is assembled using eight identical N45 neodymium ring magnets, six floating and two fixed at each end. The magnets are axially magnetized and have a 2 inch outer diameter, 0.5 inch inner diameter, and 0.25 inch height. To confine the motion of the magnets to the longitudinal (x) axis and to keep the repelling orientation (NS-SN), the magnets are placed around a circular aluminum shaft of 3/8 inch diameter, as shown in Fig. 2. To reduce the friction levels and avoid damaging the magnets through sliding contact with the aluminum shaft, a Teflon® PFA sleeve with 3/8 inch inner diameter and 1/2 inch outer diameter is pressed onto the shaft. The Teflon® sleeve was machined down in diameter to allow a loose enough fit for the magnets in order to provide low friction but tight enough fit to avoid rotation of the magnets off axis.

The n^{th} magnet is rigidly attached to the shaft; however, the rest of the magnets are free to float. The two fixed magnets are held in place by two machined aluminum cups and four threaded rods at each end. The 5/16-18 inch threaded rods allow a fine adjustment of the total length of the shock absorber, D, and enable the addition of coil windings around the magnets. The motion of the shaft, and correspondingly the n^{th} magnet, is measured by a linear variable differential transformer (LVDT) sensor and the displacements of the floating magnets are estimated utilizing a high speed Sony RX100 IV camera and a motion tracking software developed in MATLAB®.

4. PARAMETER IDENTIFICATION

For numerical analysis purposes, the parameters such as repelling force characteristics and inherent friction forces, need to be identified.

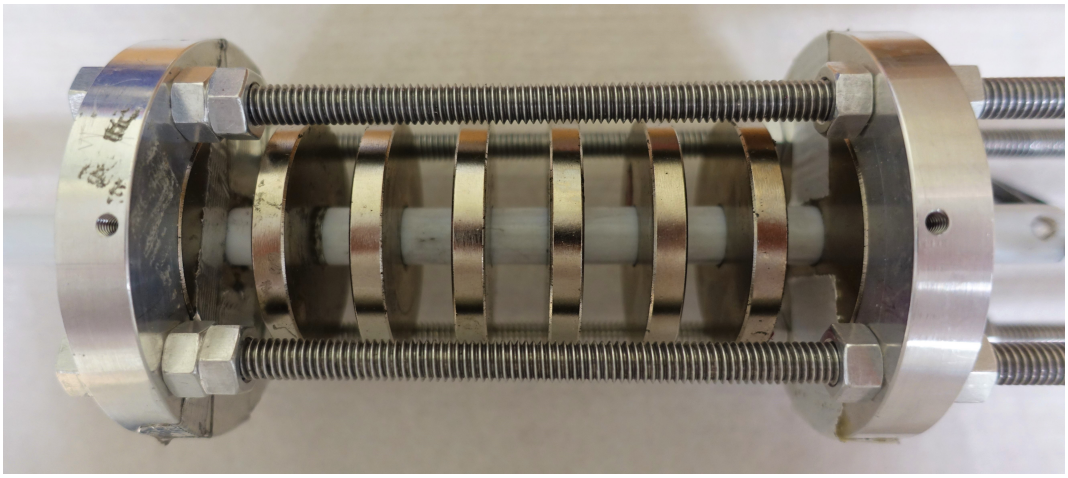

Fig. 2. Experimental apparatus of the novel shock absorber.

4.1. Repelling Force

The repelling force was determined by placing two magnets on top of each other, allowing one to float freely. Various weights were stacked on top of the floating magnet and the distance between the two magnets was recorded using the LVDT sensor. According to the curve fit in Fig. 3, the coefficients introduced in Eq.(1) were obtained to be $p = -2.151$ and $A = 6.7838 \times 10^{-3}$ N/m$^{\mathrm{p}}$.

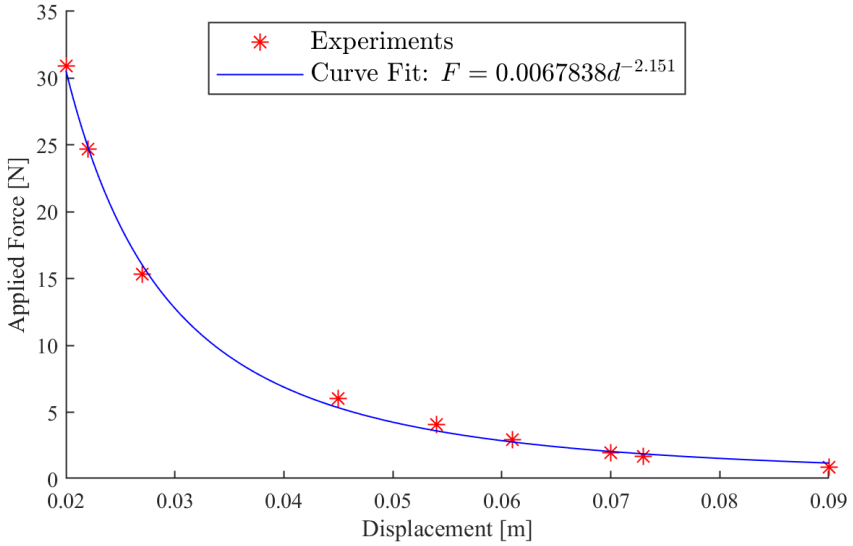

Fig. 3. Magnetic repelling force magnitude vs. displacement.

4.2. Viscous Damping

Despite the addition of the Teflon® PFA sleeve, the friction forces were still prominent in the shock absorber. To model the friction forces as a viscous damper, the damping coefficient needed to be obtained. To this end, a mass of 8.8 kg was attached to the end of the shock absorber. The mass was displaced a total of 50 mm and released. The displacement of the mass was recorded by the

LVDT sensor, as demonstrated in Fig.4. Utilizing the displacement data gathered, the logarithmic decrement was calculated using

$$\delta = \frac{1}{N-1} \ln \frac{x_1}{x_N} \tag{7}$$

where x_1 and x_N are the amplitudes of the first and the N^{th} peak [14] of the oscillation respectively. The damping ratio is then found from the logarithmic decrement using

$$\zeta = \frac{\delta}{\sqrt{(2\pi)^2 + \delta^2}} = 0.1269 \tag{8}$$

For a single degree of freedom system, the viscous damping is then obtained as

$$C_v = 2M\zeta\omega_n = 38.30 \text{ N}\cdot\text{s/m} \tag{9}$$

where M is the mass of the attached weight to the shock absorber and ω_n is the natural frequency of the free oscillating mass. Observe that this is the friction force applied to the n^{th} magnet, since the external mass is directly mounted to the shaft and the shaft is rigidly attached to the n^{th} magnet. Therefore, $C_{v_n} = C_v = 38.3$ N·s/m. This damping is due to the friction of all magnets sliding on the shaft. Therefore, the damping for each of the sliding magnets can be assumed to be $C_{v_i} = C_v/(n-1)$, (for $i = 1$ to $n-1$), since they act as dampers in series. It is to be noted, this is a simplification and due to manufacturing imperfections, the friction levels for each magnet would be slightly different; however, it offers good enough accuracy for simulation purposes.

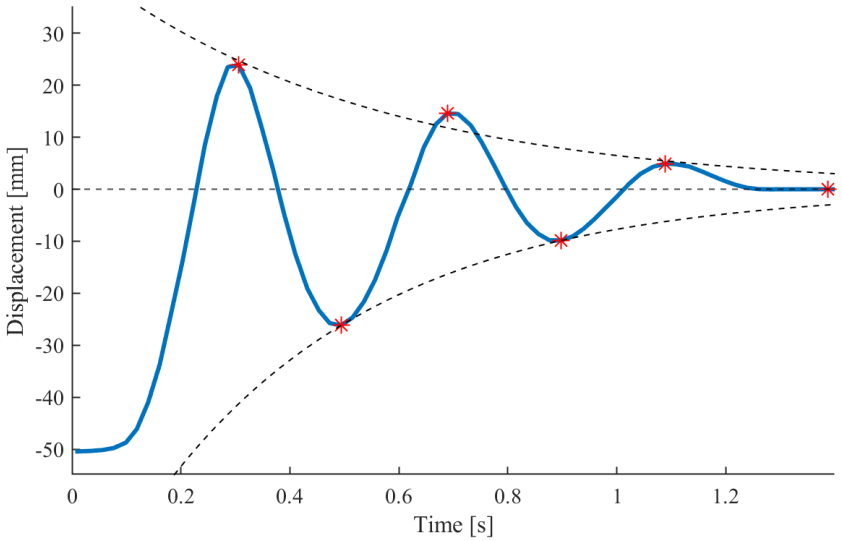

Fig. 4. Displacement of the free oscillating mass.

5. SIMULATION VERIFICATION

5.1. Stiffness

To comprehend the stiffness characteristics of the system, the force vs. displacement curve is to be generated. Experimentally, various weights having mass M were placed on the shock absorber and the static equilibrium position of the shaft, i.e. the n^{th} magnet, was recorded. For

this experiment, six moving magnets were chosen and the total length of the shock absorber was set to be $D = 14.7$ cm.

Fig. 5 summarizes the simulation and the experiment results. The simulation results followed the experimental data closely for low force values; however, the results started to deviate as the force level increased. As pointed out in the derivation of the EOM in Section 2, the forces of nonadjacent magnets were ignored. Inclusion of the attractive forces of the second adjacent magnets resulted in a more accurate simulation, as demonstrated in Fig. 5.

Since the repelling or attraction force between magnets quickly diminishes with increasing distance, ignoring the nonadjacent forces is a good approximation for low displacement. However, as the magnets get closer and closer, the interactions of the nonadjacent magnets cannot be ignored and their impact on the response of the system becomes significant. Therefore, for a more accurate simulation, these forces should be implemented in the EOM. However, inclusion of repelling force of the third adjacent magnets does not affect the results of this system significantly. The modified EOM which includes the forces of second adjacent magnets, and is utilized in the simulations is given by

$$\begin{bmatrix} m & 0 & 0 & \dots & \dots & \dots & 0 \\ 0 & m & 0 & \dots & \dots & \dots & 0 \\ 0 & 0 & \ddots & \ddots & \ddots & \ddots & \vdots \\ \vdots & \vdots & \ddots & m & \ddots & \ddots & \vdots \\ \vdots & \vdots & \ddots & \ddots & \ddots & 0 & 0 \\ \vdots & \vdots & \ddots & \ddots & 0 & m & 0 \\ 0 & 0 & \dots & \dots & 0 & 0 & m+M \end{bmatrix} \begin{Bmatrix} \ddot{x}_1 \\ \ddot{x}_2 \\ \vdots \\ \ddot{x}_i \\ \vdots \\ \ddot{x}_{n-1} \\ \ddot{x}_n \end{Bmatrix} = \tag{10}$$

$$\begin{Bmatrix} A\Big[-(d_0-x_1)^p+(d_0+x_1-x_2)^p-(2d_0+x_1-x_3)^p\Big]-C_1\dot{x}_1 \\ A\Big[(2d_0-x_2)^p-(d_0-x_2+x_1)^p+(d_0+x_2-x_3)^p-(2d_0+x_2-x_4)^p\Big]-C_2\dot{x}_2 \\ \vdots \\ A\Big[(2d_0-x_i+x_{i-2})^p-(d_0-x_i+x_{i-1})^p+(d_0+x_i-x_{i+1})^p-(2d_0+x_i-x_{i+2})^p\Big]-C_i\dot{x}_i \\ \vdots \\ A\Big[(2d_0-x_{n-1}+x_{n-3})^p-(d_0-x_{n-1}+x_{n-2})^p+(d_0+x_{n-1}-x_n)^p-(2d_0+x_{n-1})^p\Big]-C_{n-1}\dot{x}_{n-1} \\ f_n+A\Big[(2d_0-x_n+x_{n-2})^p-(d_0-x_n+x_{n-1})^p+(d_0+x_n)^p\Big]-C_n\dot{x}_n \end{Bmatrix}$$

Note that this is a hardening type of system, meaning the higher the displacement, the higher the stiffness. Using an exponential curve fitting algorithm, the force-displacement relation was estimated as

$$F(x_n) = 8.123e^{38.518x_n} + 4.185e^{-561.701x_n} \tag{11}$$

where $F(x_n)$ is the external force as a function of displacement of the n^{th} magnet, which is attached to the shaft of the shock absorber. Figure 6 shows the simulation vs the curve fit. Equation 11 can be used to quickly obtain the stiffness of the system for a given input and shows its hardening nature.

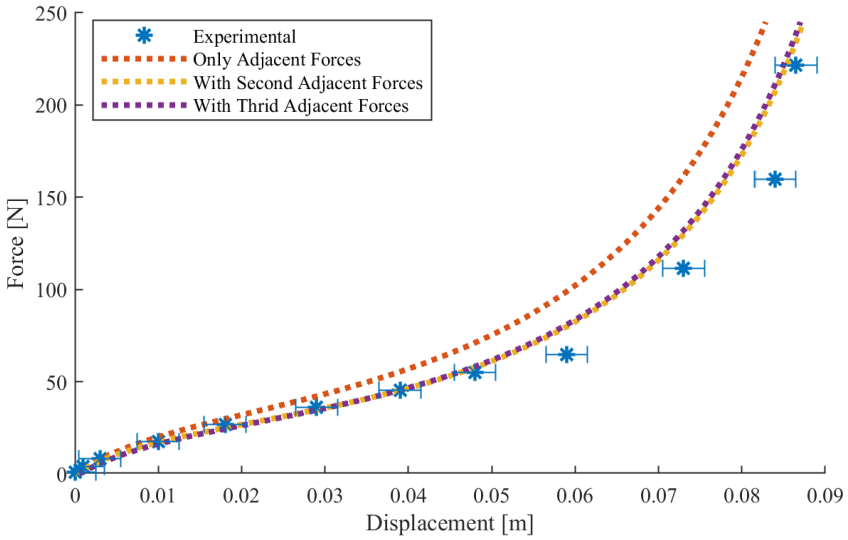

Fig. 5. Experimental and simulation results for force vs. displacement of the shock absorber.

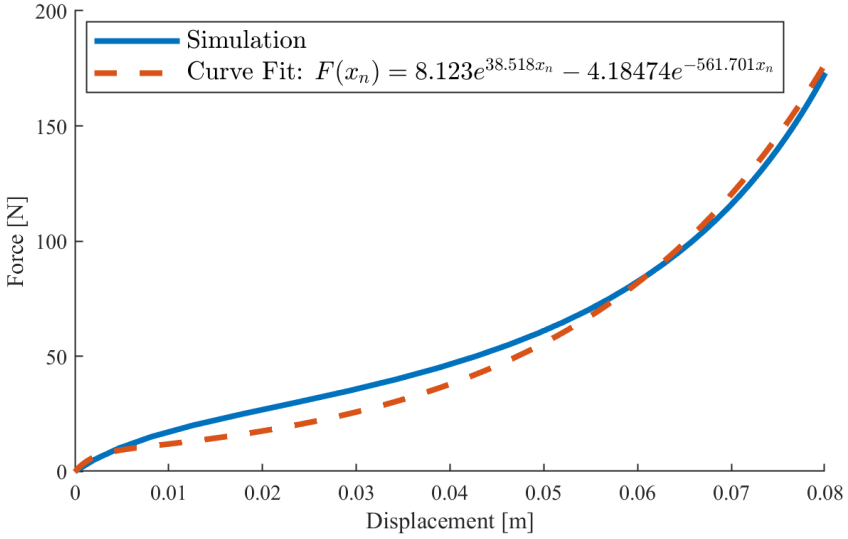

Fig. 6. Curve fit for force vs. displacement relation of the shock absorber.

5.2. Transient time response

In this section, the transient time simulation is to be validated. To do so, a mass of 2.89 kg was placed onto the shock absorber and the motion of the magnets resulting from the weight of the external mass was captured utilizing a high speed camera. Custom-developed motion tracking software was used to estimate position of individual magnets. A measuring tape was also included in the video shot for calibration of the position tracking software. In the simulation environment, the same mass was added to the shock absorber under the same conditions. The parameters used are summarized in Table 1. It is important to emphasize that in the simulation, replacing the mass with a simple constant external force with the same amplitude of the weight would be incorrect, as this would ignore the effect of inertial forces associated with the mass.

Table 1. Magnetic shock absorber parameters.

Parameter	Value	Unit
Magnet Mass, $\boldsymbol{m}$	10.5×91^{-3}	kg
Repelling Force Exponent, $\boldsymbol{p}$	-2.151	–
Repelling Force Constant, $\boldsymbol{A}$	6.784×10^{-3}	$\mathrm{N/m^p}$
Viscous Damping Coefficient, $\boldsymbol{C_v}$	38.30	$\mathrm{N \cdot s/m}$
Shock Absorber Length, $\boldsymbol{D}$	12.82	mm
Total Electrical Resistance, $\boldsymbol{R}$	0.4	Ω

The results of the camera motion tracking and the simulation are summarized in Fig. 7. The experimental data show that the magnets reach equilibrium faster than what the simulation estimates by a small amount. This is suspected to be due to the existence of stiction friction forces. A more suitable friction model that incorporates stiction forces such as the LuGre model can be utilized to further increase the accuracy of the simulation [15]. On the other hand, the motion tracking has its own shortcomings. As the magnets travel, they pass in and out of the focal point of the camera and this introduces inherent inaccuracies. However, overall the simulation and the experimental results are in good agreement.

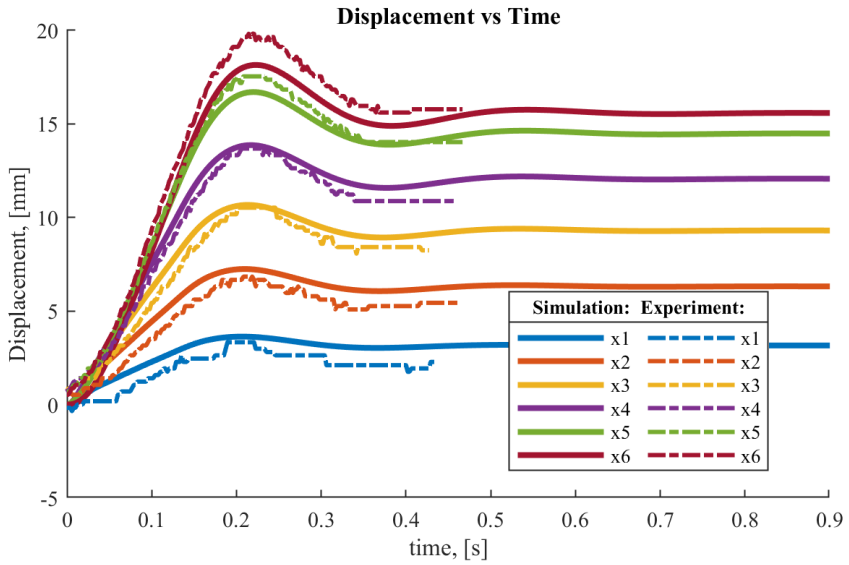

Fig. 7. Simulated and experimental displacement of each magnet in response to the weight of a 2.89 kg mass.

5.3. Coil Damping

It was proposed by [8] that the addition of electromagnetic coils will introduce damping forces and enable energy harvesting capabilities. In the experimental setup, three separate coil windings with approximately 150 turns, which were made of 24 AWG (American Wire Gauge) enameled copper wire, were added to the shock absorber. A mass of 8.8 kg was attached to the shaft and it was subjected to a sinusoidal displacement input at multiple frequencies. The test was run with and without the coils and the voltage output of the coils and the displacement of the mass were recorded. Fig. 8 shows the displacement of the mass over a range of input frequencies obtained

from the aforementioned experiment. The amplitude of displacement for the system with coils is smaller, particularly near the system's natural frequency, thereby demonstrating the effectiveness of the coils as a damper.

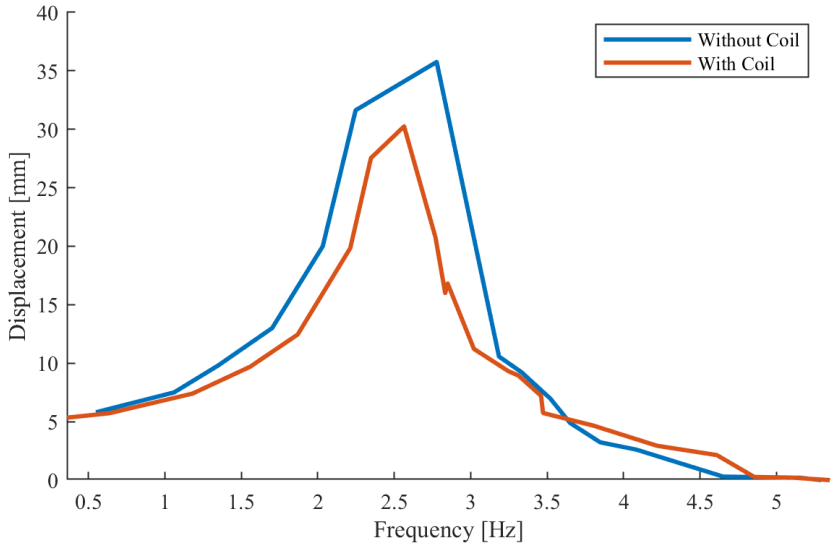

Fig. 8. Experimentally obtained displacement vs. input frequency of the free oscillating mass.

The damping forces exerted by the coils can be equated to a viscous damping by determining the energy loss. The induced currents in the coils will dissipate at a rate of V_{RMS}^2/R [16]. Therefore, a Discrete Fourier Transform (DFT) was conducted on the voltage output of the coils and the sinusoidal function of the voltage output was reconstructed. Fig 9 demonstrates the experimental voltage output and the DFT reconstruction for one of the coils in response to a sinusoidal displacement input to the shock absorber. Through the DFT reconstruction, the voltage can be represented by a sum of multiple alternating voltages as

$$V(t) = \sum_{j=1}^{q} V_j \cos(\omega_j t + \psi_j) \tag{12}$$

where q is the number of terms used to reconstruct the DFT, V_j is the amplitude of the j^{th} term, and ω_j and ψ_j are the frequency and phase of the j^{th} term, respectively. Utilizing Eq.(12), the energy dissipated in one cycle can be determined to be

$$E_{dissipated} = \Delta t P_{avg} = \Delta t \sum_{j=1}^{q} \frac{V_{RMS_j}^2}{R} \tag{13}$$

where P_{avg} is the average electric power generated by the induced current in the coils, $V_{RMS_j} = V_j/\sqrt{2}$ is the root mean square voltage of the j^{th} alternating voltage, R is the electrical resistance of the coil, $\Delta t = 2\pi/\omega$ is the duration of one cycle of system oscillation, and ω is the input frequency. On the other hand, the energy dissipated by a viscous damper during a single cycle in a harmonic oscillator can be obtained as

$$E_v = \int_0^{\Delta t} F_v \, dx = \int_0^{2\pi/\omega} F_v \dot{x} \, dt \tag{14}$$

where $F_v = -c_{eq}\dot{x}$ is the force exerted by the viscous damper, $\dot{x} = \omega X_0 \cos(\omega t)$ is the velocity of the mass, X_0 is the amplitude of the oscillation, and c_{eq} is the equivalent viscous damping coefficient. As a result,

$$E_v = -c_{eq} \int_0^{2\pi/\omega} \dot{x}^2 \, dt = -c_{eq} \pi \omega X_0^2 \tag{15}$$

Therefore, equating the energy dissipated by the coils, $E_{dissipated}$, to the energy dissipated by a damper, the equivalent damping coefficient can be obtained by

$$c_{eq} = \frac{\sum_{j=1}^{q} V_j^2}{R\omega^2 X_0^2} \tag{16}$$

For simulation efficiency, the coil damping can be simplified to a viscous damper as given in Eq. 16, which depends on the voltage and displacement amplitude, input frequency, and the electric resistance.

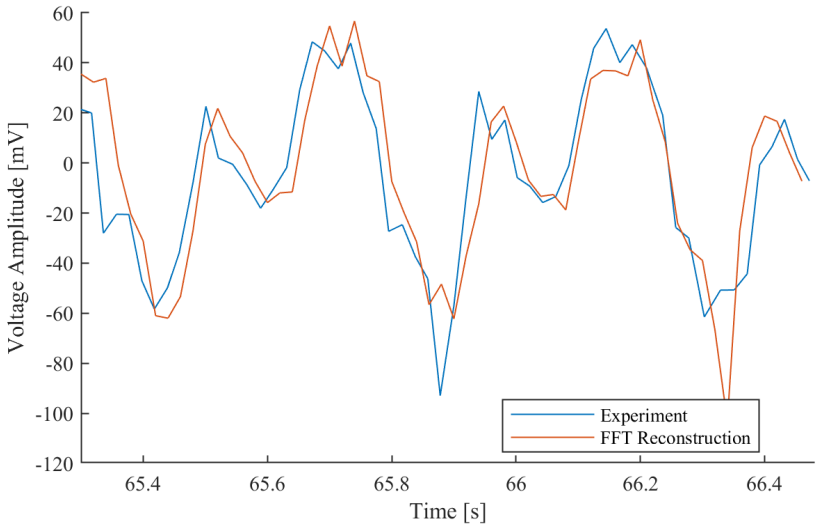

Fig. 9. Voltage output of the top coil to a 1.8 Hz sinusoidal displacement excitation.

6. CONCLUSIONS

In this paper, the derived dynamics of the novel shock absorber element proposed by [8] were validated experimentally. Utilizing the manufactured shock absorber, the parameters such as repelling force and friction forces needed for the simulation were identified. The obtained parameters were then used to simulate various experiments. Firstly, the stiffness of the element was obtained and the developed EOM were modified to further increase the accuracy of the simulation. It was shown that the stiffness of the system is exponential in nature which in automotive suspension systems can be designed to combine the relatively low initial stiffness, to absorb minor road undulations and increase grip, and transition to a secondary higher stiffness, to improve vehicle roll control during cornering. Then, the simulated transient time response of the system was compared to experimental results which were obtained by tracking the motion of the individual magnets using computer vision. The dynamic simulation results followed the experimental results closely validating the correctness of the EOM and the assumptions. Lastly, it was shown that the electromagnetic

coils act as an energy dissipation source, producing an alternating current which can be converted to direct current by a bridge rectifier to be easily stored in a battery system. It was demonstrated that the damping due to coils can be modelled as a viscous damper for simulation efficiency. This magnetic shock absorber can be implemented in road and rail vehicle suspension systems, replacing conventional viscous dampers which behave in a time-variant way due to dependence on viscous fluid temperature. The element also has the potential for developing energy harvesting systems or active suspension systems through energization of the electromagnetic coils.

REFERENCES

1. Ruzicka, J.E. and Derby, T.F. *Influence of Damping in Vibration Isolation.* United States Government Printing Office, 1971.
2. Karnopp, D. "Active and semi-active vibration isolation." *Journal of mechanical design*, Vol. 117, No. 2, pp. 177–85, 1995.
3. Rabinow, J. "The magnetic fluid clutch." *Transactions of the American Institute of Electrical Engineers*, Vol. 26, No. 2, pp. 1308–15, 1948.
4. Sassi, S., Cherif, K., Mezghani, L., Thomas, M. and Kotrane, A. "An innovative magnetorheological damper for automotive suspension: from design to experimental characterization." *Smart Materials and Structures*, Vol. 14, No. 4, pp. 811–22, 2005.
5. Laalej, H., Lang, Z.Q., Sapinski, B. and Martynowicz, P. "MR damper based implementation of nonlinear damping for a pitch plane suspension system." *Smart Materials and Structures*, Vol. 21, No. 4, pp. 1–14, 2012.
6. Case, D., Taheri, B. and Richer, E. "Multiphysics modeling of magnetorheological dampers." *The International Journal of Multiphysics*, Vol. 7, No. 1, pp. 61–76, 2013.
7. Dyke, S.J., Spencer, B.F., Sain, M.K. and Carlson, J.D. "Modeling and control of magnetorheological dampers for seismic response reduction." *Smart Materials and Structures*, Vol. 5, No. 5, pp. 565–75, 1996.
8. Daliri Shadbad, A., Langlois, R.G., Khouli, F. and Afagh, F.A. "Simulation and characterization of a novel nonlinear magnetic shock absorber element." *Manuscript accepted for publication in Proceedings of the Canadian Society of Mechanical Engineering International Congress*, 2023.
9. Moleron, M., Leonard, A. and Daraio, C. "Solitary waves in a chain of repelling magnets." *Journal of Applied Physics*, Vol. 155, No. 18, 2014.
10. Spreemann, D., Hoffmann, D., Folkmer, B. and Manoli, Y. "Numerical optimization approach for resonant electromagnetic vibration transducer designed for random vibration." *Journal of Micromechanics and Microengineering*, Vol. 18, No. 10, 2008.
11. Stephen, N.G. "On energy harvesting from ambient vibration." *Journal of Sound and Vibration*, Vol. 293, No. 1, pp. 409–25, 2006.
12. Beeby, S.P., Torah, R.N., Tudor, M.J., Glynne-Jones, P., O'Donnell, T., Saha, C.R. and Roy, S. "A micro electromagnetic generator for vibration energy harvesting." *Journal of Micromechanics and Microengineering*, Vol. 17, No. 7, pp. 1257–65, 2007.
13. Chiu, M., Chang, Y., Yeh, L. and Chung, C. "Numerical assessment of a one-mass spring-based electromagnetic energy harvester on a vibrating object." *Archives of Acoustics*, Vol. 41, No. 1, pp. 119–31, 2016.
14. Thomson, W.T., and Dahleh, M.D. *Theory of Vibration with Applications.* 5 ed.. Prentice Hall, 1998.
15. Flores, P. "Comparison of different contact force models for low and moderate impact velocities: Numerical and experimental analysis." *New Trends in Mechanism and Machine Science*, pp. 549–56, 2012.
16. Sodano, H.A., Bae, J., Inman, D.J. and Belvin, W.K. "Improved concept and model of eddy current damper." *Journal of Vibration and Acoustics*, Vol. 128, No. 3, pp. 294–302, 2006.